Published by
NIGERIAN SOCIETY OF PHYSICAL SCIENCES
Available online @ https://journal.nsps.org.ng/index.php/jnsps

J. Nig. Soc. Phys. Sci. 7 (2025) 2326

Journal of the Nigerian Society of Physical Sciences

Zn(II) and Fe(II) complexes of 2,4-dinitro-N-[(Z)-[(E)-3-(2-nitrophenyl)prop-2-enylidene] amino] aniline: synthesis, characterization and *In Silico* SARS-CoV-2 inhibition studies

K. O. Eberendu[a,*], J. I. Iheanyichukwu[b], O. M. Mac-kalunta[b], C.I. Nwankwo[c], I. E. Otuokere[b], J. C. Nnaji[b]

[a]*Department of Chemistry, Spiritan University, Nneochi, Abia, Nigeria*
[b]*Department of Chemistry, Michael Okpara University of Agriculture, Nigeria*
[c]*Department of Biochemistry, Michael Okpara University of Agriculture, Nigeria*

Abstract

The hydrazones and their metal complexes find application as anticancer, antibacterial, chemotherapeutic, antioxidants, and antiproliferative agents, among several other uses. In our quest for possible bioactive hydrazone and complexes, we have synthesized novel Zn(II) and Fe(II) metal complexes of 2,4-dinitro-N-[(Z)-[(E)-3-(2-nitro-phenyl) prop-2-enylidene] amino. The octahedral geometry of the complexes was further supported by the spectral methods, with coordination proceeding through two nitro groups, two chloride atoms, an NH group, and an azomethine nitrogen atom. From the fact noted, we can now confirm that Zn(II) and Fe(II) can coordinate DNEAA to form complexes of high stability. The molecular docking study showed binding energies to be above -9.6 Kcal/mol. These results recommend biological, preclinical, and clinical trials take place, with the target being SARS-CoV-2 protease.

DOI:10.46481/jnsps.2025.2326

Keywords: Complexes, Zinc, Iron, SARS-CoV-2, Molecular docking

Article History :
Received: 24 August 2024
Received in revised form: 16 September 2024
Accepted for publication: 09 November 2024
Available online: 07 January 2025

Communicated by: Aderonke A. Oloidi

1. Introduction

Hydrazones and their metal complexes play a very enormous role in covering various fields like cytotoxicity, analytical chemistry, catalysis, optoelectronics, photoresponse, biomedicine, and wastewater cleanup in aquatic bodies [1]. Furthermore, they have had applications in some areas, including antioxidants, chemotherapeutic drugs, antibacterial, and antiproliferative. Hydrazones with their various metal complexes have found diverse uses with inorganic chemistry, materials science, Langmuir films, and, moreover, electrochemical sensors or strong enhancement in bioactivity [1]. A general push for diverse benefits that have been seen in the preparation of metallic complexes [2–18]. These ligands have shown a strong biological influence and have been tested in various stimulatory,

*Corresponding author: Tel.: +234-706-529-7631.
Email address: ifeanyiotuokere@gmail.com (K. O. Eberendu)

anticancer, and antibacterial activities [17, 18]. Medicinal importance had already been discovered in transition metal complexes [17, 18].

SARS-Cov-2 showed very high infectious properties and could easily and rapidly be transmitted between humans via droplets or from direct contact sources [19]. A new Corona virus had emerged at the end of 2019 [20]. The onset of this disease was followed by the COVID-19 pandemic, which raised international concern because of the high-level pollution, fast infectivity, and high mortality rates. The causing agent of COVID-19 is a beta coronavirus that is 89.1% related to the SARS-CoV [21]. Measures to control the spread of the virus were imposed [22]. Studies have shown that chloroquine (CQ) and hydroxychloroquine (HCQ), which are antimalarial and autoimmune medicines, can inhibit viral infection by raising the pH levels in endosomes. On this basis, the FDA has approved the usage of these medicines [23–26]. Combination therapy consisting of Remdesivir (RDV) and its active metabolites has shown a highly effective means of restraining the replication of SARS-CoV-2 in various studies on its clinical efficacy [27–29]. Arbadol, generic name umifenovir, is an antiviral medication that inhibits the binding of viruses to the host cell. It is active against a wide spectrum of various classes of viruses. It is currently in clinical trials to prove its effectiveness against COVID-19 [30, 31]. Major attention was paid to the virtual screening of the potential compounds capable of efficiently suppressing the deleterious effects of SARS-CoV-2 by computational chemists.

Several hydrazones and their complexes have been synthesized and studied for medicinal properties [1, 2, 15, 17]. To the best of our knowledge, the synthesis of Zn(II) and Fe(II) complexes of DNEAA hydrazone is reported for the first time. This study utilized *in silico* methods to analyze a novel aniline hydrazone, DNEAA, and its Zn(II) and Fe(II) complexes. The aim of the current research is to evaluate the drug-likeness of DNEAA and its Zn(II) and Fe(II) complexes for use as a pharmacological alternative in the inhibition of the deleterious effects of the SARS-CoV-2 NSP1 protein. This knowledge is applicable to structure-based drug design, allowing the molecule to be used as a template for synthesizing novel inhibitors and repurposing other compounds.

2. Materials and methods

2.1. Synthesis of DNEAA

This reaction was conducted using only analytical-grade chemicals and reagents imported from Sigma Aldrich and used without further treatment. The chemicals used were 2, 4-dinitrophenylhydrazine and 3-(2-nitrophenyl)prop-2-enal. DNEAA was prepared as in literature, with slight modification [13, 32]. To the clear solution, obtained by filtering a warm mixture of 1.99 g (0.01 mol.) of 2,4-DNP, 10 mL of concentrated H_2SO_4, 15 mL of water, and 25 mL of methanol, 1.77 g (0.01 mol.) of the carbonyl compound 3-(2-nitrophenyl)prop-2-enal was added and heated just to boiling for 10 minutes (Figure 1a). The precipitates formed were allowed to cool to room temperature before they were recrystallized from methanol and dried in a desiccator.

2.2. Synthesis of [Zn(DNEAA)Cl_2] and [Fe(DNEAA)Cl_2]

The [Zn(DNEAA)Cl_2] and [Fe(DNEAA)Cl_2] were prepared using methods described by Prushan [33]. Exactly 1.36 g (0.01 mol) of $ZnCl_2$ was dissolved in 5 ml of methanol; the mixtures were stirred for 5 minutes. The solution of the DNEAA ligand was obtained by dissolving 3.57 g (0.01 mol) of the newly synthesized compound in a hot solution of methanol solvent, which was added to the solution of the metal salts, stirred, cooled, and finally recrystallized with methanol solvent and dried at room temperature. The same procedure was repeated with 1.27 g of $FeCl_2$. Equations of reactions are shown in equations (1) and (2).

$$[ZnCl_2] + DNEAA \rightarrow [Zn(DNEAA)Cl_2]. \quad (1)$$

$$[FeCl_2] + DNEAA \rightarrow [Fe(DNEAA)Cl_2]. \quad (2)$$

2.3. Physical measurements

Melting points in open capillaries were determined using Mettler Toledo's MT 211 melting point apparatus from Mettler Company. Elemental analysis was determined using an EA 2400 Series II analyzer. A solubility check was carried out in common solvents (DMF, DMSO, water, ethanol, and methanol) at 25 °C using 1 g. Molar conductances were measured using Orion Star A212 Conductivity Bench Meter.

2.4. Characterization

The UV/visible spectra of DNEAA and the complexes were recorded on a Shimadzu UV-1800 UV-Vis spectrophotometer. DMSO was used as solvent. The infrared spectra were recorded using a Perkin-Elmer (Model C91158) IR spectrophotometer with the "KBr Pellet Technique." The NMR spectrum was recorded using a JEOL GSX-400 spectrometer. DMSO-d_6 was used as solvent.

2.5. Molecular docking

The crystal structure of NSP1 from SARS-CoV-2 (PDB ID: 7K3N) was obtained from the RCSB Protein Databank. The water molecules were effectively eliminated using ArgusLab 4.0.1 software [34]. The DNEAA, [Zn(DNEAA)Cl_2] and [Fe(DNEAA)Cl_2] were drawn with ChemDraw version 18.0 from PerkinElmer Informatics [35] and then converted to PDB using ArgusLab 4.0.1. Software [34]. The molecular docking simulations were conducted using the PyRx open-source software, employing the Auto Dock Vina tool [36]. The receptor was uploaded and converted to a macromolecule. The DNEAA, [Zn(DNEAA)Cl_2] and [Fe(DNEAA)Cl_2] were uploaded using the Open Babel option embedded in PyRx software [36]. The virtual screening was conducted using Vina wizards. A Vina search was conducted to encompass the region of the compounds' top domain where they interact with the 7K3N receptor. Upon completion of virtual screening, PyRx automatically proceeded to the analysis results page, where the computed results of virtual screening were presented. Auto Dock Vina automatically generated the nine most optimal binding modes for each ligand. The mode with the highest binding energy for

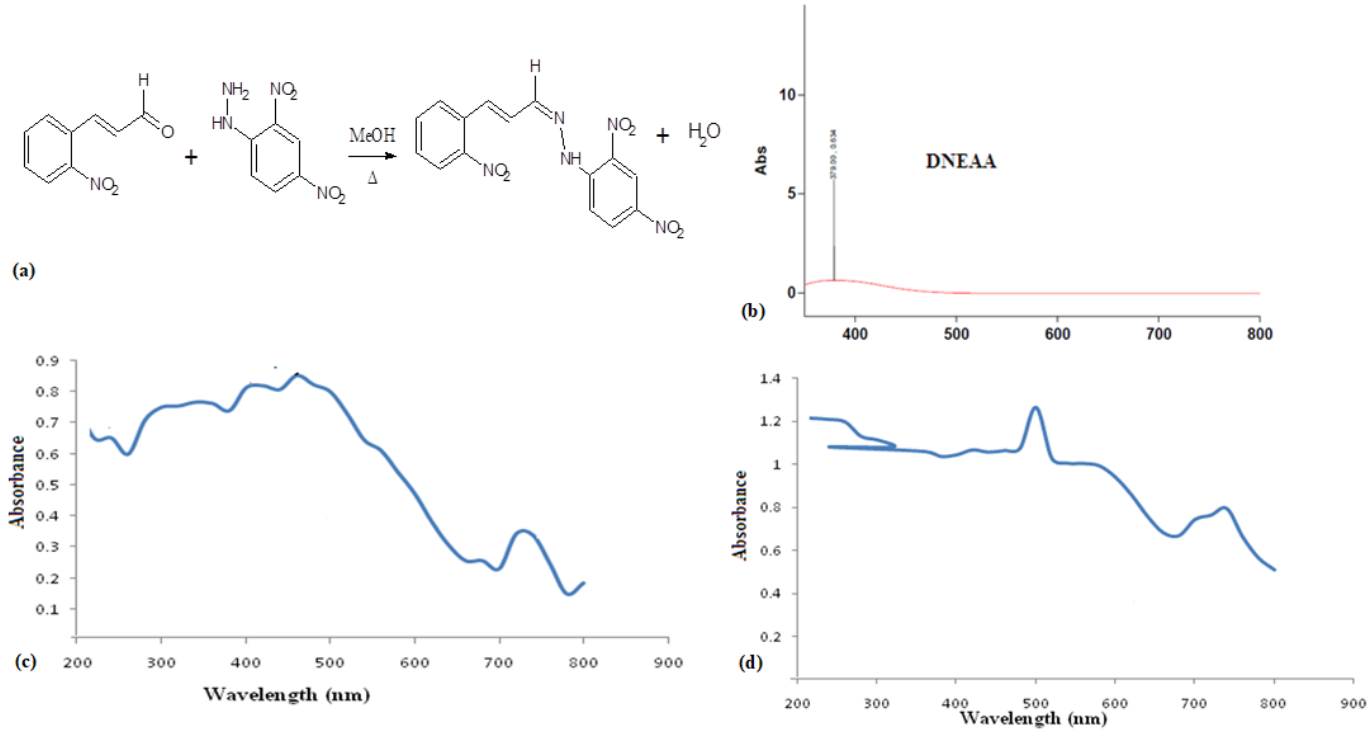

Figure 1. (a) Synthesis of DNEAA (b) Electronic spectrum of DNEAA (c) Electronic spectrum of [Zn(DNEAA)Cl2] (d) Electronic spectrum of [Fe(DNEAA)Cl2].

Table 1. Physical properties of DNEAA, $[Zn(DNEAA)Cl_2]$ and $[Fe(DNEAA)Cl_2]$.

Compounds	Colour	M.P(°C)	Yield (%)	Found (calc.) (%)		
				C	H	N
DNEAA	Yellowish-red	115	91	50.40(50.43)	3.50(3.10)	19.90(19.60)
$[Zn(DNEAA)Cl_2]$	White	260	93	37.00(36.50)	2.32(2.25)	14.24(14.90)
$[Fe(DNEAA)Cl_2]$	Green	190	83	37.20(37.22)	2.26(2.29)	14.49(14.47)

Table 2. Molar conductivity and solubilities of DNEAA, $[Zn(DNEAA)Cl_2]$ and $[Fe(DNEAA)Cl_2]$.

Compounds		Solubility Ratings (25 ^{0}C)				
	Molar conductivity ($Ohm^{-1}cm^2mol^{-1}$)	DMF	DMSO	Water	Ethanol	Methanol
DNEAA	-	3	3	2	2	2
$[Zn(DNEAA)Cl_2]$	56	3	3	1	1	1
$[Fe(DNEAA)Cl_2]$	47	3	3	1	1	1

Note: 3 = Very soluble, 2 sparingly soluble and 1= insoluble.

Table 3. Electronic spectral data of DNEAA, $[Zn(DNEAA)Cl_2]$ and $[Fe(DNEAA)Cl_2]$.

Compounds	$\pi - \pi^*$(nm)	LMCT (nm)	$T_{2g} \rightarrow E_g$ (nm)
DNEAA	379	-	-
$[Zn(DNEAA)Cl_2]$	260	430, 470	750
$[Fe(DNEAA)Cl_2]$	286	511	755

each ligand was chosen for secondary study. Azythromycin, the reference drug, was also docked to 7K3N as a control to validate the docking protocol. The visualization of the docked complexes was performed using the protein-ligand interaction profiler server [37].

3. Results and discussion

Physical properties of DNEAA and its metal complexes are presented in Table 1. The ligand and its Fe complex are

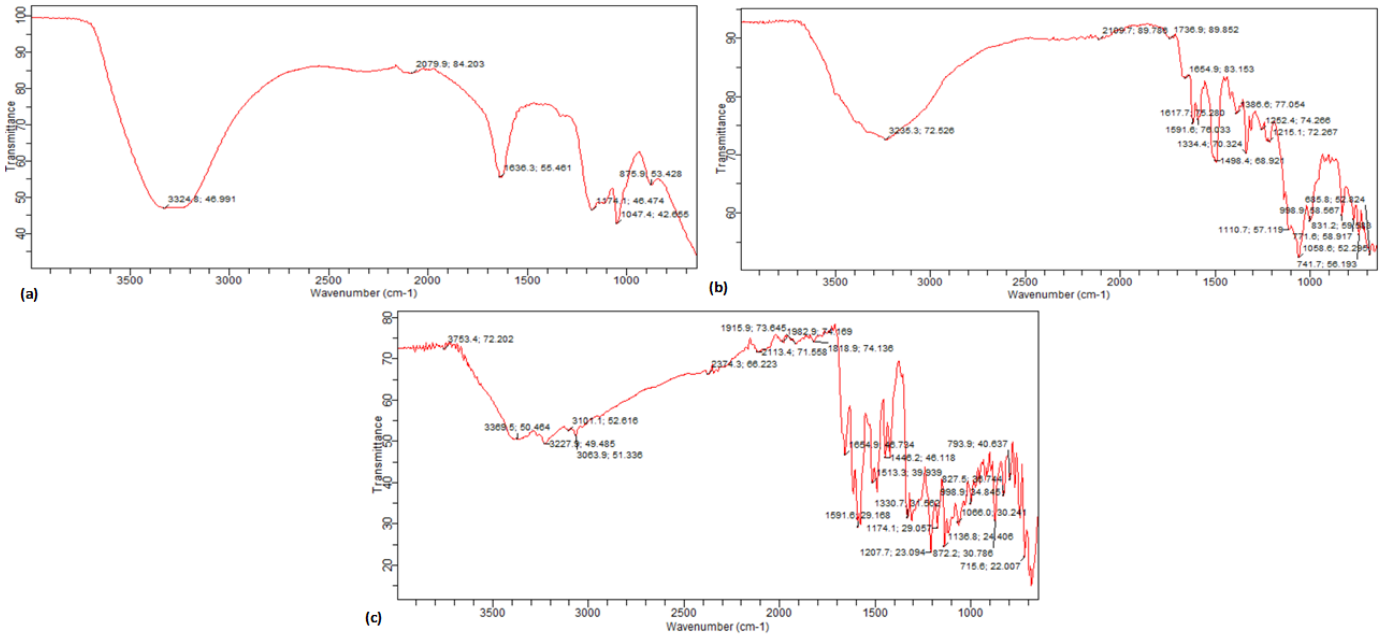

Figure 2. (a) FTIR spectrum od DNEAA (b) FTIR spectrum of [Zn(DNEAA)Cl_2] (c) FTIR spectrum of [Zn(DNEAA)Cl_2].

Table 4. Selected FTIR spectral data DNEAA and its metal complexes.

Functional Group	DNEAA	[Zn(DNEAA)Cl_2]	[Fe(DNEAA)Cl_2]
=C-H (Ar) bending.	900.1	831.2	872.2
N-H	3324.8	3235.3	3369.5
Ar-NO_2	1353.3	1334.4	1330.7
>C=N	1636.3	1617.8	1591.6
M-N	-	741.7	715.6
M-Cl	-	654.2	651.9

coloured, crystalline, and air-stable at room temperature. In contrast, the zinc complex is white in colour, although it belongs to the category of transition metals. This occurs as Zinc's d orbitals are fully occupied with electrons, meaning that an electron can never make a d→d transition as no state is available. They are soluble in both DMF and DMSO, but not soluble in water, ethanol and methanol (Table 2). The percentage yield of the synthesized hydrazone is 91% and those of the metal complexes are ([Zn(DNEAA)Cl_2]) 93% and ([Fe(DNEAA)Cl_2]) 83%. This can be the reason for ascertaining that the methods used in synthesizing were effective. The determined melting points are indicated in Table 1. The molar conductance of all the tested complexes of DNEAA, as shown in Table 2, lies in the range of non-electrolytes (56 and 47 $Ohm^{-1}cm^2mol^{-1}$) for the Zn and Fe complexes, respectively. Thus, confirmation of anionic coordination to the complexing metal ions [38].

3.1. *Electronic spectra of the DNEAA, [Zn(DNEAA)Cl_2] and [Fe(DNEAA)Cl_2]*

Electronic transitions for DNEAA and its metal complexes are presented in Table 3. The electronic spectra are shown in Figures 1a-c. The UV-visible spectra were recorded in DMSO. DMSO typically absorbs UV light at a low absorbance at a wavelength of 270 nm [39].This absorption peak is due to the n→π* transition of the sulfoxide group [39]. Its weak absorbance is especially important to note since the presence of DMSO in a system will cause barely any signal variation. Importantly, DMSO does not induce significant changes in the shapes or intensities of the spectral features of compounds dissolved in it. Because of this, DMSO can be used in UV-Vis spectroscopic applications without concern for obtaining "clean" data.

The band at 379 nm in the spectrum of the DNEAA is assigned the π→π* transition of the azomethine moieties [40]. This transition is generally defined as an intra-ligand charge transfer (ILCT), and in the spectra of the metal complex, it was displaced to shorter wavelengths ([Zn(DNEAA)Cl_2]) 260 nm and ([Fe(DNEAA)Cl_2]) 286 nm . The shifting of the wavelengths of the bands is because of the coordination of the DNEAA ligand with the different metal centres [40]. These indicated the formation of an M-L coordination bond [41]. For the [Zn(DNEAA)Cl_2], the bands at 430 and 470 nm represent the ligand-to-metal charge transition (LMCT). The band at 750 nm in [Zn(DNEAA)Cl_2] was assigned to T_{2g}→E_g transition. For the [Fe(DNEAA)Cl_2], the band at 511 nm was assigned to the LMCT and 755 nm was due to the T_{2g}→E_g transition, suggesting a d6 octahedral complex [42]. Our study on the electronic spectra agreed well with the report of Edozie *et al*. [6]. They reported that ILCT, LMCT, and d-d transitions were observed in the electronic spectral of metal complexes.

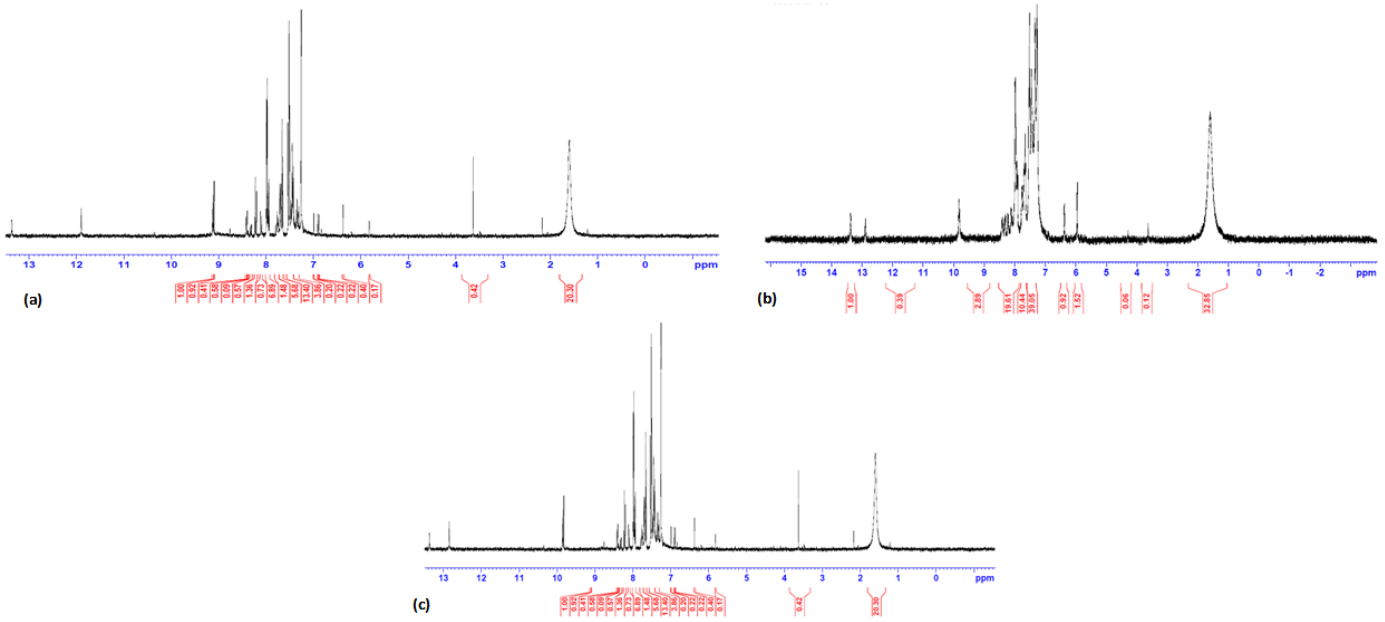

Figure 3. (a) $_1$HNMR spectrum of DNEAA (b) $_1$HNMR spectrum of [Zn(DNEAA)Cl_2] (c) $_1$HNMR spectrum of [Fe(DNEAA)Cl_2].

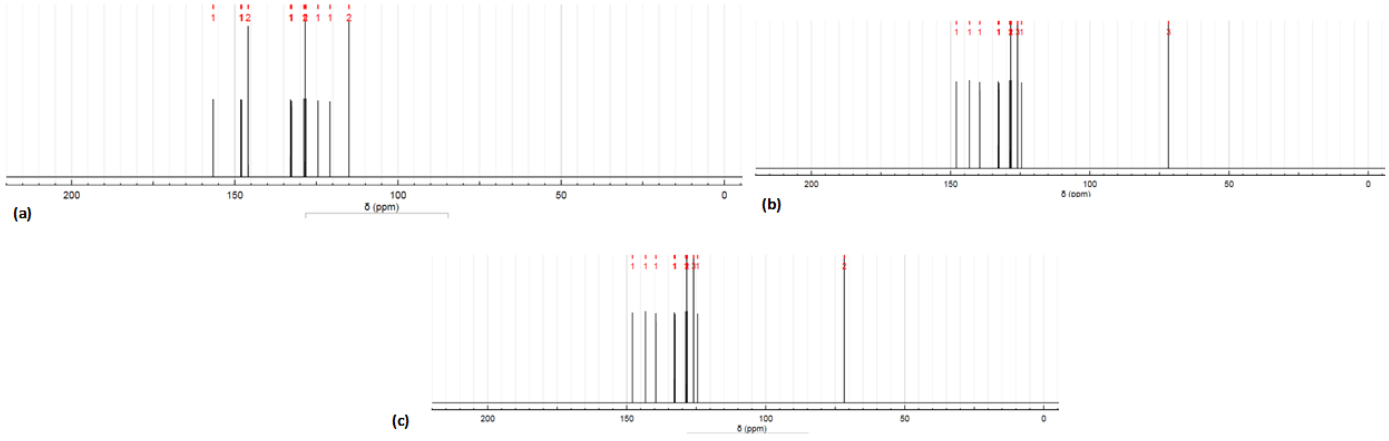

Figure 4. (a) $_{13}$C-NMR spectrum of DNEAA (b) $_{13}$C-NMR spectrum of [Zn(DNEAA)Cl_2] (c) $_{13}$C-NMR spectrum of [Fe(DNEAA)Cl_2].

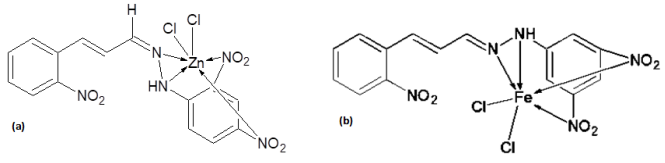

Figure 5. (a) Proposed structures for [Zn(DNEAA)Cl_2] (b) Proposed structure for [Fe(DNEAA)Cl_2].

3.2. Infrared spectra of the DNEAA and its metal complexes

Selected FTIR peaks of the DNEAA and its complexes are shown Table 4. Figures 2a –2c represents the FTIR spectra of the DNEAA, [Zn(DNEAA)Cl_2] and [Fe(DNEAA)Cl_2] respectively.

Comparisons of FTIR spectra between DNEAA and metal complexes were made. The broad band at 3324.8 cm^{-1} was assigned to the stretching frequency of hydrogen bonding of the NH group of the ligand. The vibration of this frequency was very much lowered in the spectra of [Zn(DNEAA)Cl_2] (3235.3 cm^{-1}) and was increased in the spectrum of [Fe(DNEAA)Cl_2] (3369.5 cm^{-1}), respectively. This indicated that the complexation was through the NH group. Increased electron density increased the N-H bond length and consequently slowed down the vibration frequency in [Zn(DNEAA)Cl_2]. Structural vibrations of the -CH group of the ligand and metal complexes were vibrated at a frequency range of 920.7–872.2 cm^{-1}. Strong peaks observed at a frequency range of 1636.3 cm^{-1} corresponded to the vibrations of the -C=N group of the ligand. Lowering of frequency to 1617.8 and 1591.6 cm^{-1} in the complexes suggested that the azomethine group was actively involved in coordination [40]. An increase in electron density increased C=N bond length and consequently retarded the vibration frequency. These vibrations due to M-N, signifying coordination,

Table 5. Selected ^{1}HNMR spectral data of DNEAA, [Zn(DNEAA)Cl_2] and [Fe(DNEAA)Cl_2].

Compounds	(ppm)			
	N=C-H	H–C=C	Ar-H	N-H
DNEAA	9.1, s, 1H	6.4, d, 2H	7.5-8.5, m, 7H	11.9, s,1H
[Zn(DNEAA)Cl_2]	9.9, s, 1H	6.5, d, 2H	7.8-8.5, m, 7H	12.9, s, 1H
[Fe(DNEAA)Cl_2]	9.9, s, 1H	6.0, d, 2H	7.7-8.5, m, 7H	12.9, s, 1H

d = doublet, m = multiplet, s = singlet

Table 6. Selected ^{13}C-NMR spectral data of DNEAA, [Zn(DNEAA)Cl_2] and [Fe(DNEAA)Cl_2].

Compound	C=C Ar (1) (ppm)	C=C Ar (2) (ppm)	C=C Conj. Alkene (ppm)	C=N- Azomethine (ppm)
DNEAA	124.5-147.9	115.9-148.1	128.4-132.9	157.6
[Zn(DNEAA)Cl_2]	124.5-147.9	71.7-139.5	128.4	146.2
[Fe(DNEAA)Cl_2]	124.5-147.9	71.7-139.5	128.4	146.2

Table 7. Binding affinities and interactions of DNEAA, [Zn(DNEAA)Cl_2] and [Fe(DNEAA)Cl_2] with SARS-CoV-2.

Compound	Binding Affinity Kcal/mol	Hydrophobic interactions	Hydrogen bonding
DNEAA	-10.3	LEU 12A, GLN 13A, VAL 14A, GLU 46A	VAL 11A, GLN 13A, VAL 14A, GLU 46A
Zn(DNEAA) Cl_2	-9.9	GLN 13A, VAL 14A,	VAL 14A, GLN 13A, ARG 15A, GLN 54A
Fe(DNEAA) Cl_2	-9.6	GLN 13A, VAL 14A, VAL 11A, GLU 46A	VAL 14A, GLU 46A
Azithromycin	-6.4	-	SER 63C, SER 64C, GLY 64C, GLY 66C, GLN 67C, HIS 69C

were attributed to the lower frequency bands observed at 741.7 and 715.6 cm^{-1} [43]. Similar shifts suggesting coordination were also observed by Asogwa and Otuokere [43]. They reported that M-N bonds occurred in the far infrared regions [43]. The bands at the lower regions of the spectra 654.2 and 651.9 cm^{-1} are the M-Cl vibrational frequencies of the ligand, which showed that the Cl^{-} were involved in the coordination [43].

3.3. NMR of the DNEAA and its metal complexes

The ^{1}H NMR chemical shifts of the DNEAA, [Zn(DNEAA)Cl_2] and [Fe(DNEAA)Cl_2] are shown in Table 5. The ^{1}H NMR spectra are shown in Figures 3a–c.

The signal of the azomethine proton (-HC=N-) was observed at 9.1 ppm in the spectrum of DNEAA. In the spectra of the complexes, the signal was shifted downfield to 9.9 ppm. This implied involvement of the azomethine proton in the complexation. This is in agreement with the report of Asogwa and Otuokere in their report on Fe(II) and Cu(II) nano-sized complexes of sulfamethoxazole [43]. The peaks to the aromatic protons are observed as multiplet peaks at 7.5 to 8.0 ppm in the ligand and complexes. In addition, a deshielding effect exists in the C=C bond plane due to π-electron anisotropy and steric effects [42]. Together, these explained the signals that appear at δ = 6.0-7.0 ppm, which correspond to the protons bound to the olefinic carbon (H-C=C-H). The peak due to N-H (11.9 ppm) appeared deshielded because of electronegative nitogen. This peak was also shifted to 12.9 ppm in the spectra of the complexes. The electron density around the NH proton reduced as the NH group formed complexes with the Zn(II) and Fe(II) ions. The deshielding effect shifted the NH proton's resonance to a lower field, which consequently caused a downfield shift with a high value in ppm of the NMR spectrum. This shift therefore indicated that the N-H proton participated in complexation. Secondly, the multiplets at the 7.5-8.4 ppm range are an indication that there exist two aromatic rings (7H) in the DNEAA and complexes whose protons resonated at 7.50, 7.60, 7.95, 8.10, 8.20, 8.30 and 8.40 ppm. The hygroscopic nature of DMSO lead to a substantial water peak at 3.63 ppm (DNEAA), 3.61 ppm ([Zn(DNEAA)Cl_2]), and 3.61 ppm ([Fe(DNEAA)Cl_2]) in proton NMR spectrum.

The ^{13}C NMR spectral data of DNEAA, [Zn(DNEAA)Cl_2] and [Fe(DNEAA)Cl_2] are summarized in Table 6. The C-13 spectra are shown in Figures 4a–4c.

The signal at δ 157.6 ppm was attributed to the carbon atom attached to the azomethine group in DNEAA. In the spectra of the corresponding metal complexes, the chemical shift res-

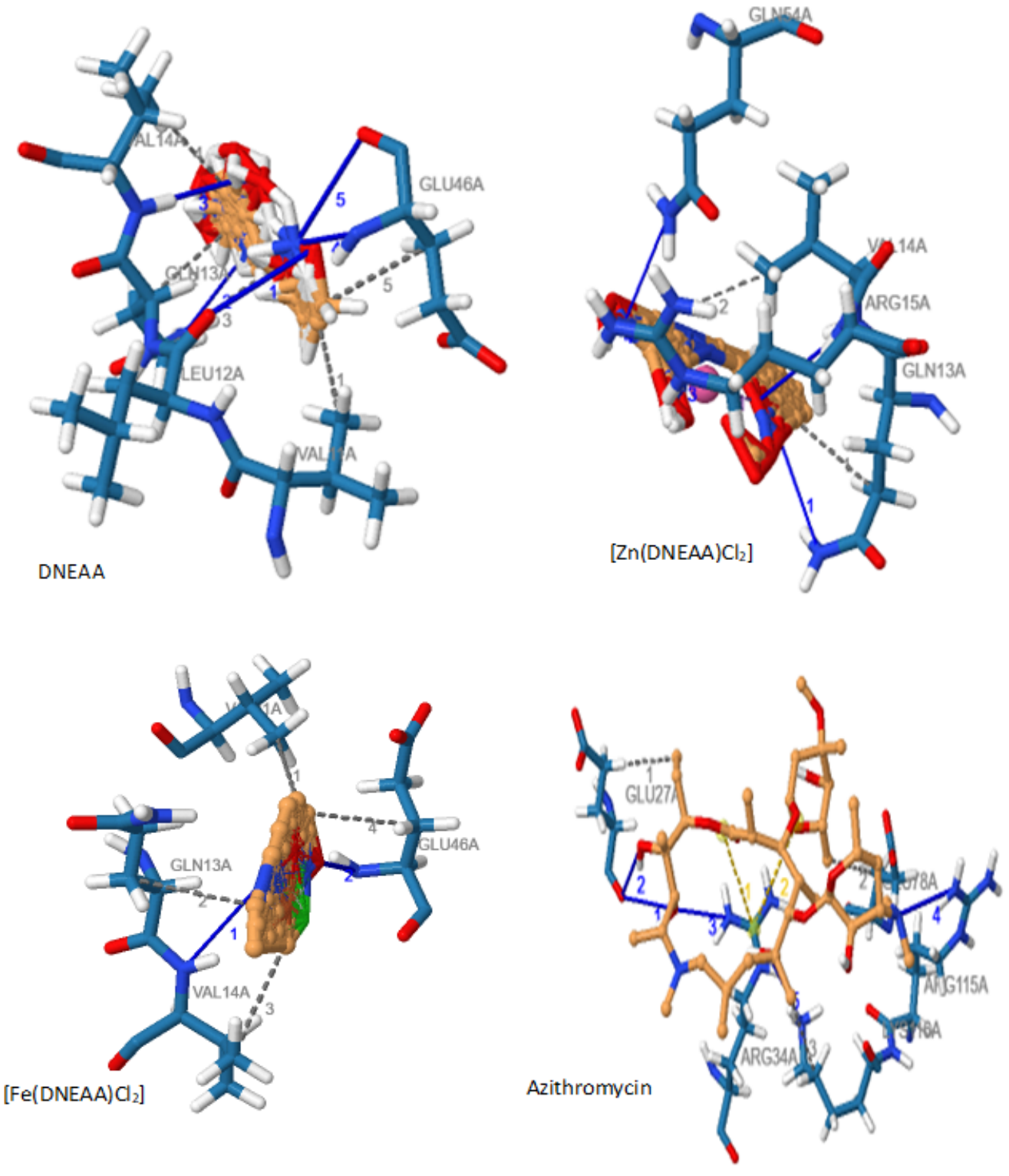

Figure 6. (a) Proposed structure of $[Zn(DNEAA)Cl_2]$ (b) Proposed structure of $[Fe(DNEAA)Cl_2]$.

onated at δ 146.2 ppm. This seemed to advance that the nitrogen atom of the azomethine group coordinated with the central metal ion. The coordination of the ligand to the different metals was confirmed by a new peak observed at 125.9 ppm, which is absent in the ligand spectrum. Similar reports were also documented by Edozie *et al*. [6]. For both the ligand and the complexes, the aromatic ring carbons resonated at 124.5–147.9 ppm. In a ^{13}C NMR spectrum, the signal for $DMSO_{-d6}$

typically appears around 39.5 ppm. This peak corresponds to the carbon atoms in the DMSO$_{-d6}$ molecule. In our spectra (Figures 4a–4c), the DMSO$_{-d6}$ peaks were not visible. This has been attributed to lesser sensitivity of ^{13}C NMR compared to ^{1}H NMR and solvent suppression techniques that was used.

Based on spectroscopic information, the structures shown in Figures 5a and b have been proposed for the [Zn(DNEAA)Cl$_2$] and [Fe(DNEAA)Cl$_2$] complexes, respectively.

The binding affinities and interactions of DNEAA and its metal complexes with SARS-CoV-2 are shown in Table 7. The 3D interactions are shown in Figure 6.

The computed binding affinities (Table 7) demonstrated that DNEAA and its complexes can effectively inhibit the SARS-CoV-2 protease. The binding affinities were better than the FDA approved drug, azithromycin. The DNEAA ligand and its metal complexes were shown to interact with SARS-CoV-2. The 3D interactions of the DNEAA and its metal complexes with SARS-CoV-2 have been shown in Figure 6.The interaction of amino acids and compounds at the allosteric binding sites has been summarized in Table 7. For DNEAA, hydrophobic interactions have been found to be at a distance of 3.48, 3.67, 3.72, 3.94, and 3.73 Å for LEU 12A, GLN 13A, VAL 14A, and GLU46A. Also, hits were observed at VAL 11A, GLN 13A, VAL 14A, and GLU 46A with bond distances of 3.34, 3.23, 2.66, 3.17, and 3.56 Å, respectively, for hydrogen bond interactions. Similar interactions consisting of a substituted phenyl ring connected to the conjugated azomethine group of the hydrazone ligand have also been reported [44].

Hydrophobic interactions for the [Zn(DNEAA)Cl$_2$] complex were observed at fragment hits GLN 13A and VAL 14A at a distance of 3.71 and 3.82 Å, respectively, while hydrogen bonding interactions were observed at a distance of 3.38, 4.05, 3.48, and 3.29 Å at VAL 14A, GLN 13A, ARG 15A, and GLN 54A. The interactions of [Fe(DNEAA)Cl$_2$] also showed hits with the hydrogen-bonding fragment for 7K3N. The hydrophobic interaction was seen at 3.53 Å for GLN13A, 3.72 Å for VAL14A, 3.54 Å for VAL11A, and 3.73 Å for GLU46A. Hydrogen bonding was noted at distances of 4.01 for VAL 14A and 3.13 Å for GLU 46A.

According to the analysis of the 3D interactions, hydrogen bonding, which is a characteristic marker of strong interactions between proteins and ligands and frequently results in increased binding affinity, was found to be less prevalent than hydrophobic interactions. Usually, an increase in the amount of H-bonds in such interactions increases the inhibitory potential towards the target [25]. Singh *et al.* [45] noted that the binding affinity score of azithromycin with SARS-CoV-2 was -6.9 kcal/mol, while that of hydroxychloroquine was -5.7 kcal/mol. In agreement with our work, the binding energies derived from the docking of the SARS-CoV-2 protein with DNEAA, [Zn(DNEAA)Cl$_2$], and [Fe(DNEAA)Cl$_2$] were -10.3, -9.9, and -9.6 kcal/mol, respectively.

4. Conclusion

Synthesis and characterization of DNEAA, [Zn(DNEAA)Cl$_2$], and [Fe(DNEAA)Cl$_2$] were done. The metal complexes were characterized based on the observed FTIR spectra, electronic spectra, melting point, solubility, proton, and carbon-13 nuclear magnetic resonance. An octahedral structure was proposed for the complexes. The ability of DNEAA to chelate Zn(II) and Fe(II) is hereby assured. Molecular docking results showed that DNEAA and its complexes have the tendency to inhibit SARS-CoV-2 protease. Following these results, it is recommended to carry out further investigations concerning the protease of SARS-CoV-2 along with the *in vitro*, *in vivo*, preclinical, and clinical trials.

Data availability

We do not have any research data outside the submitted manuscript file.

References

[1] K. Mishra, S. Goswami, M.V. Kumudhavalli, K. Saini, N. Pal, N. Sharma & P. Pandey, "Hydrazones and their metal complexes: A short review on their biological potential", International Journal of Research in Pharmaceutical Sciences **11** (2020) 1440. https://doi.org/10.26452/ijrps.v11iSPL4.4319.

[2] T. Arora, J. Devi, A. Boora & S. Rani,"Synthesis and characterization of hydrazones and their transition metal complexes: antimicrobial, antituberculosis and antioxidant activity", Research in Chemical Intermediate **49** (2023) 4819. https://doi.org/10.1007/s11164-023-05116-1.

[3] S. K. Mondal, W. Chenglin, F. C. Nwadire, A. Rownaghi, A. Kumar, Y. Adewuyi & M.U. Okoronkwo, "Examining the effect of a chitosan biopolymer on alkali-activated inorganic material for aqueous Pb (II) and Zn (II) sorption", Langmuir **38** (2022) 903. https://doi.org/10.1021/acs.langmuir.1c01829.

[4] I. E. Otuokere, J. G. Ohwimu, K. C. Amadi, C. O. Alisa, F. C. Nwadire, O. U. Igwe, A. A. Okoyeagu & C. M. Ngwu,"Synthesis, characterization and molecular docking studies of Mn (II) complex of sulfathiazole", Journal of Nigerian Society of Physical Sciences **1** (2019) 95. https://doi.org/10.46481/jnsps.2019.20.

[5] I. E. Otuokere, D. O. Okorie, B. C. Asogwa, O. K. Amadi, l. O. C. Ubani & F. C. Nwadire, "Spectroscopic and Coordination Behavior of Ascorbic Acid Towards Copper (II) Ion", Research in Analytical and Biological Chemistry **1** (2017) 1. https://dx.doi.org/10.4314/jasem.v26i1.12.

[6] I. O. Edozie, O. J. Godday, A. K. Chijioke, I. O. Uchenna & N. F. Chigozie, "Synthesis, characterization and molecular docking studies of Co (II) metal complex of sulfathiazole", Bulletin of Chemical Society of Ethiopia **34** (2020) 83. https://doi.org/10.4314/bcse.v34i1.8.

[7] I. E. Otuokere, L. O. Okpara, K. C. Amadi, C. O. Alisa, A. Okoyeagu & F. C. Nwadire, "4-N-(7-Chloroquinolin-4-yl)-1-N, 1-N-diethyl petane-1, 4-diamine Ti Complex: Synthesis and Characterization", BP International (2021) 142. https://doi.org/10.9734/bpi/tipr/v3/1827E.

[8] J. Godwin, F. C. Nwadire & B. A. Uzoukwu, "Extraction of Ni (II) Ions into $CHCl_3$ Solution of n, n'-Ethylenebis (4-Butanoyl-2, 4-Dihydro-5-Methyl-2-Phenyl-3h-Pyrazol-3-One Imine) Schiff Base", European Chemical Bulletin **1** (2012) 269. https://doi.org/10.17628/ECB.2012.1.269-273.

[9] I. E. Otuokere, K. C. Nwaiwu, F. C. Nwadire & O. U. Akoh, "Synthesis and characterization of Cr (III)-ascorbic acid complex", Journal of Applied Science and Environmental Management **26** (2022) 75. https://doi.org/10.4314/jasem.v26i1.12.

[10] I. E. Otuokere, L. O. Okpara, K. C. Amadi, N. Ikpo, G. U. Okafor & F. C. Nwadire, "Synthesis, Characterization And Complexation Of Cr(III) Ion Using Chloroquine Diphosphate", Journal of Chemical Society of Nigeria **49** (2019) 107. https://journals.chemsociety.org.ng/index.php/jcsn/article/view/254.

[11] O. K. Amadi, I. E. Otuokere & C. F. Bartholomew, "Synthesis, Characterization, *in vivo* Antimalarial Studies and Geometry Optimization

of Lumefantrine/Artemether Mixed Ligand Complexes", Research Journal of Pharmaceutical Dosage Forms and Technology **7** (2015) 59. DOI: https://doi.org/10.5958/0975-4377.2015.00009.9.

[12] I. E. Otuokere, K. C. Nwaiwu, F. C. Nwadire & O. U. Akoh, "Synthesis and characterization of Cr (III)-ascorbic acid complex", Journal of Applied Science and Environmental Management **26** (2022) 75. https://doi.org/10.4314/jasem.v26i1.12.

[13] I. E. Otuokere, B. C. Asogwa, F. C. Nwadire, O. U. Akoh, C. I. Nwankwo, P. O. Emole & E. E. Elemike, "Biological Potentials of Some Schiff Bases and Their Chelates: A Short Review", in *Novelties in Schiff Bases*, Takashiro Akitsu (Ed.), IntechOpen, London, United Kingdom, 2024, pp. 140-158. https://doi.org/10.5772/intechopen.114862.

[14] F. C. Nwadire, C. O. Ubani, I. E. Otuokere, O. U. Igwe, J. N. Chilaka & H. O. Chukwuemeka, "Effects of acids, anions and auxiliary complexing species on the distribution of bivalent nickel in liquid-liquid extraction", Journal of Chemical Society of Nigeria **44** (2019) 661. https://journals.chemsociety.org.ng/index.php/jcsn/article/view/319.

[15] N. P. Belskaya, W. Dehaen, V. A. Bakulev, "Synthesis and properties of hydrazones bearing amide, thioamide and amidine functions", Archive of Organic Chemistry **1** (2010) 275. http://dx.doi.org/10.3998/ark.5550190.0011.108.

[16] N. M. Abdul Khader Jailani, A. Xavier, A. Ramu, "Synthesis, Spectroscopic Characterization, DNA Binding Ability and Biological Activities of Transition Metal Complexes Containing Tridentate Schiff base", Materials Today: Proceedings **5** (2018) 22200. https://doi.org/10.1016/j.matpr.2018.06.585.

[17] J. Wahbeh & S. Milkowski, "The Use of Hydrazones for Biomedical Applications", SLAS Technology **24** (2019) 161. https://doi.org/110.1177/2472630318822713.

[18] X. Wang, Y. Jaun, S. LI, Z. Guoping & S. Baoan, "Design, synthesis, and antibacterial activity of novel Schiff base derivatives of quinazolin-4(3H)-one", European Journal of Medicinal Chemistry **22** (2014) 65. https://doi.org/10.1016/j.ejmech.2014.02.053.

[19] P. Zhai, Y. Ding, X. Wu, J. Long, Y. Zhong & Y. Li, "The epidemiology, diagnosis and treatment of COVID-19", International Journal of Antimicrobial Agents **55** (2020) 105955. https://doi.org/10.1016/j.ijantimicag.2020.105955.

[20] Y. Guo, Q. D. Cao, Z. S. Hong, Y. Y. Tan, S. D.Chen, H.J. Jin, K.S. Tan, D.Y. Wang & Y. Yan, "The origin, transmission, and clinical therapies on coronavirus disease 2019 (COVID-19) outbreak an update on the status", Mil Medicinal Research **7** (2020) 11. https://doi.org/10.1186/s40779-020-00240-0.

[21] J. H. Beigel, K. M.Tomashek, L. E. Dodd, A. K. Mehta, B. S. Zingman, A. C. Kalil, E. Hohmann, H. Y. Chu, A. Luetkemeyer, S. Kline, D. Lopez de Castilla, R. W. Finberg, K. Dierberg, V. Tapson, L. Hsieh, T. F. Patterson, R. Paredes, D. A. Sweeney, W. R. Short, G. Touloumi, "Remdesivir for the Treatment of Covid-19 Final Report", The New England Journal of Medicine **383** (2020) 1813. https://doi.org/10.1056/NEJMoa2007764.

[22] A. Y. Lai, L. Lee, M. P. Wang, Y. Feng, T. T. Lai, L. M. Ho, V. S. Lam, M. S. Ip & T. H. Lam, "Mental Health Impacts of the COVID-19 Pandemic on International University Students, Related Stressors, and Coping Strategies", Frontiers Psych **11** (2020) 584240. https://doi.org/10.3389/fpsyt.2020.584240.

[23] C. A. Devaux, J. M. Rolain, P. Colson & D. Raoult, "New insights on the antiviral effects of chloroquine against coronavirus: what to expect for COVID-19?", International Journal of Antimicrobial Agent **55** (2020) 105938. https://doi.org/10.1016/j.ijantimicag.2020.105938.

[24] F. Touret & X. de Lamballerie, "Of chloroquine and COVID-19", Antiviral. Research **177** (2020) 104762. https://doi.org/10.1016/j.antiviral.2020.104762

[25] M. Al-Bari, "Targeting endosomal acidification by chloroquine analogs as a promising strategy for the treatment of emerging viral diseases", Pharmacology Research Perspective **5** (2017) 293. https://doi.org/10.1002/prp2.293.

[26] M. E. Rebeaud & M. F. Zores, "SARS-CoV-2 and the use of chloroquine as an Antiviral Treatment, "Frontiers in Medicine **7** (2020) 7. https://doi.org/10.3389/fmed.2020.00184.

[27] J. A. Al-Tawfiq, A. H. Al-Homoud & Z. A. Memish, "Remdesivir as a possible therapeutic option for the COVID-19", Travel Medicinal Infectious Diseases **10** (2020) 16. https://doi.org/10.1016/j.tmaid.2020.101615.

[28] J. S. Morse, T. Lalonde, S. Xu & W. R. Liu, "Learning from the Past: Possible Urgent Prevention and Treatment Options for Severe Acute Respiratory Infections Caused by 2019-nCoV", European Journal of Chemistry and Biology **21** (2020) 730. https://doi.org/10.1002/cbic.202000047.

[29] T. P. Sheahan, A. C. Sims, S. Zhou, R. L. Graham, A. J. Pruijssers, M. L. Agostini, S. R. Leist, A. Schäfer, L. J. Dinnon, J. D. Stevens, X. Chappell, T. M. Lu, A. S. Hughes, C. S. George, S. A. Hill, S. A. Montgomery, A. J. Brown, G. R. Bluemling, M. G. Natchus, M. Saindane & R. S. Baric, "An orally bioavailable broad-spectrum antiviral inhibits SARS-CoV-2 in human airway epithelial cell cultures and multiple coronaviruses in mice", Science trans. Medicine **12** (2020) 5883. https://doi.org/10.1126/scitranslmed.abb5883.

[30] D. He, S. Zhao, X. Xu, Q. Lin, Z. Zhuang, P. Cao, M. H. Wang, Y. Lou, L. Xiao, Y. Wu & L. Yang, "Low dispersion in the infectiousness of COVID-19 cases implies difficulty in control", BMC Public Health **20** (2020) 1558. https://doi.org/10.1186/s12889-020-09624-2.

[31] Y. S. Boriskin, I. A. Leneva, E. I. Pécheur & S. J. Polyak, "Arbidol: a broad-spectrum antiviral compound that blocks viral fusion", Current Medicinal Chemistry **15** (2008) 997. https://doi.org/10.2174/092986708784049658.

[32] I .E. Otuokere & A. J. Chinweuba, "Synthesis, Characterization and fungicidal activity of 3-chloro-4-methyl-N-[(1E)-1-phenylethylidene]aniline ligand and its metal complexes", Journal of Chemical and Pharmaceutical Research **6** (2011) 905. https://www.jocpr.com/articles/synthesis-characterization-and-fungicidal-activity.

[33] M. J. Prushan, "Lab Manual Advanced Inorganic Chemistry Laboratory", Department of Chemistry and Biochemistry, La Salle University, Philadelphia, Pennsylvania, 2003. http://www1.lasalle.edu/~prushan/Inorganic%20Lab%20Manual.pdf

[34] M. Bouhdada, M. El Amane, H. El Hamdani & Z. Khiya, "Synthesis, characterization, biological evaluation and molecular docking studies of salicylidene-aniline and their metal mixed ligand complexes with caffeine", Journal of Molecular Structure **1271** (2023) 134026. https://doi.org/10.1016/j.molstruc.2022.134026.

[35] B. A. Ismail, D. A. Nassar, Z. H. Abd El-Wahab & O. A. M Ali, "Synthesis, characterization, thermal, DFT computational studies and anticancer activity of furfural-type Schiff base complexes", Journal of Molecular Structure **1227** (2021) 129393. https://doi.org/10.1016/j.molstruc.2020.129393.

[36] P. A. Khalf-Alla, S. S. Hassan & M. M. Shoukry, "Complex formation equilibria, DFT, docking, antioxidant and antimicrobial studies of iron(III) complexes involving Schiff bases derived from glucosamine or ethanolamine", Inorganic Chimical Acta **492** (2019) 192. https://doi.org/10.1016/j.ica.2019.04.035.

[37] F. Rahaman, P. Gupta, M.N. Manjunatha & P. Gautam, "Benzo [g] indole-based Schiff's base ligand and its transition metal complexes: Synthesis, characterization and anti-microbial activity studies", Materials Today Proceedings **62** (2022) 5598. https://doi.org/10.1016/j.matpr.2022.04.814

[38] B. C. Asogwa & I. E. Otuokere, "Sonochemical synthesis and characterization of Fe(II) and Cu(II) nano-sized complexes of sulfamethoxazole", Journal of Nigerian Society of Physical Sciences **6** (2024) 2011. https://doi.org/10.46481/jnsps.2024.2011.

[39] M. M. R. Badal, H. Z. Hossain & M. Maniruzzaman, "Synthesis, identification and computational studies of novel Schiff bases *N*-(2,6-dibenzylidenecyclohexylidene)-*N′*-(2,4-dinitrophenyl)hydrazine derivatives", SN Applied Sciences **2** (2020) 1914. https://doi.org/10.1007/s42452-020-03745-4.

[40] M. A. Thompson, "Molecular docking using ArgusLab, an efficient shape-based search algorithm and the AScore scoring function", ACS meeting Philadelphia **172** (2004) 42. https://doi.org/10.1007/978-1-4939-9752-7_13.

[41] P. A. Khalf-Alla, S. S. Hassan & M. M. Shoukry, "Complex formation equilibria, DFT, docking, antioxidant and antimicrobial studies of iron(III) complexes involving Schiff bases derived from glucosamine or ethanolamine", Inorganica Chimica Acta **492** (2019) 192. https://doi.org/10.1016/j.ica.2019.04.035.

[42] S. Dallakyan & A. J. Olson, "Small-molecule library screening by docking with PyRx", In Chemical Biology **1263** (2015) 243. https://doi.org/10.1007/978-1-4939-2269-7_19.

[43] S. Salentin, S. Schreiber, V. J. Haupt, M. F. Adasme & M. Schroeder,

"PLIP: fully automated protein-ligand interaction profiler", Nucleic Acids Research **43** (2015) W443. https://doi.org/10.1093/nar/gkv315.

[44] J. Singh, D. Malik & A. Raina, "Molecular docking analysis of azithromycin and hydroxychloroquine with spike surface glycoprotein of SARS-CoV-2", Bioinformation **17** (2021) 11. https://doi.org/10.6026/97320630017011.

[45] J. Singh, D. Malik & A. Raina,"Molecular docking analysis of azithromycin and hydroxychloroquine with spike surface glycoprotein of SARS-CoV-", Bioinformation **17** (2021) 11. https://doi.org/10.6026/97320630017011.